Scripta Materialia 199 (2021) 113897

Contents lists available at ScienceDirect

Scripta Materialia

journal homepage: www.elsevier.com/locate/scriptamat

Anomalous size effect in micron-scale CoCrNi medium-entropy alloy wire

Jin-Xi Chen[a,b], Yan Chen[a,b,*], Jun-Peng Liu[a], Tian-Wei Liu[a,b], Lan-Hong Dai[a,b,c,*]

[a] State Key Laboratory of Nonlinear Mechanics, Institute of Mechanics, Chinese Academy of Sciences, Beijing 100190, China
[b] School of Engineering Science, University of Chinese Academy of Sciences, Beijing 101408, China
[c] State Key Laboratory of Explosion Science and Technology, Beijing Institute of Technology, Beijing, 100081, China

ARTICLE INFO

Article history:
Received 22 February 2021
Accepted 22 March 2021
Available online 1 April 2021

Keywords:
Medium-entropy alloy wire
Size effect
Strain gradient
Multiple deformation twins

ABSTRACT

Micron-sized CoCrNi medium-entropy alloy (MEA) wires are successfully fabricated by Taylor-Ulitovsky method for the first time. The wires of two different sizes, with diameters of 40 and 100 microns, exhibit an excellent combination of tensile strength and ductility. In-depth microstructure characterization indicates the superior mechanical properties stem from the synergy of Lomer-Cottrell locks, mechanical nano-twinning and HCP stacking. Surprisingly, an anomalous size effect is presented in the tension of these microwires, i.e., the much higher tension strength and ductility are observed in the 40 micron-wire, in sharp contrast to conventional single-principal element alloys only showing negligibly minor tension size effect. Much higher density of geometrically necessary dislocation accompanying heterogeneous deformation is observed in 40 micron-wire, leading to a high strain gradient, which is in turn joined with multiple deformation twins giving rise to high strength and ductility in 40 micron-wire.

Microwires, such as conventional single-principal element alloy microwires [1,2], shape memory alloy microwires [3–5], and amorphous alloy microwires [6], play an irreplaceable role in the field of precise instruments and advanced manufacturing technologies. To achieve higher accuracy and reliability, small diameter, high strength and sufficient ductility are all urgently required. However, it was found that diameter influence on tension behavior was negligibly minor in most traditional microwires [1], and high strength is usually combined with low ductility, e.g. typical pearlitic steel wire could reach super-high strength by means of fiercely sacrificing its ductility [7]. Hence, how to explore microwires with both smaller diameter and better performance is still a challenging problem.

During past decade, material systems with multiple principal elements in equi-molar or near-equimolar ratio, called high-entropy alloys (HEAs) or medium-entropy alloys (MEAs), have attracted wide interests [8–17]. The unique design concept endow these alloys unexpected mechanical properties and giant potential to overcome traditional strength-ductility trade-off dilemma [18–21], including exceptional fracture toughness at cryogenic temperature [22,23], excellent performance under extreme conditions, e.g., extraordinary self-sharpening ability [24], which broaden our horizons to solve many intractable problems existing in traditional materials. Most previous researches were focused on bulk materials, only several pioneering works have been made in H/MEA millimeter-wires [25–27]. Nevertheless, micron-sized H/MEA wires have not been reported yet. In this work, CoCrNi MEA was selected as raw material due to its outstanding mechanical properties [28–33]. The CoCrNi microwires of two different sizes, with diameters of 40 and 100 microns, were successfully fabricated by using Taylor-Ulitovsky method [34]. These microwires possess excellent combination of strength and ductility. Surprisingly, these microwires exhibit an anomalous size effect on tensile behavior. The underlying mechanisms of this anomalous size effect were revealed by a series of microstructure characterizations combined with quantitative analysis.

Ingots of equimolar CoCrNi MEA were prepared by arc melting from pure metals of 99.9 wt.% purity and were re-melted four times to ensure composition homogeneities. The sample with a diameter of 4.5mm and a length of 10mm was cut from bulk ingot as feedstock. Microwires with lengths of 200mm were fabricated by the Taylor-Ulitovsky equipment. Glass shell was removed by dilute hydrofluoric acid corrosion after fabrication.

Specimens with a gauge length of 15mm were tested on a dynamical mechanical analyzer (DMA Q800) by using tension film clamp at room temperature. The sample was fixed to a paper frame with a rectangular hole at center, and the paper frame was cut off when tensile tests started. The tensile tests were performed at

* Corresponding authors.
E-mail addresses: chenyan@lnm.imech.ac.cn (Y. Chen), lhdai@lnm.imech.ac.cn (L.-H. Dai).

https://doi.org/10.1016/j.scriptamat.2021.113897
1359-6462/

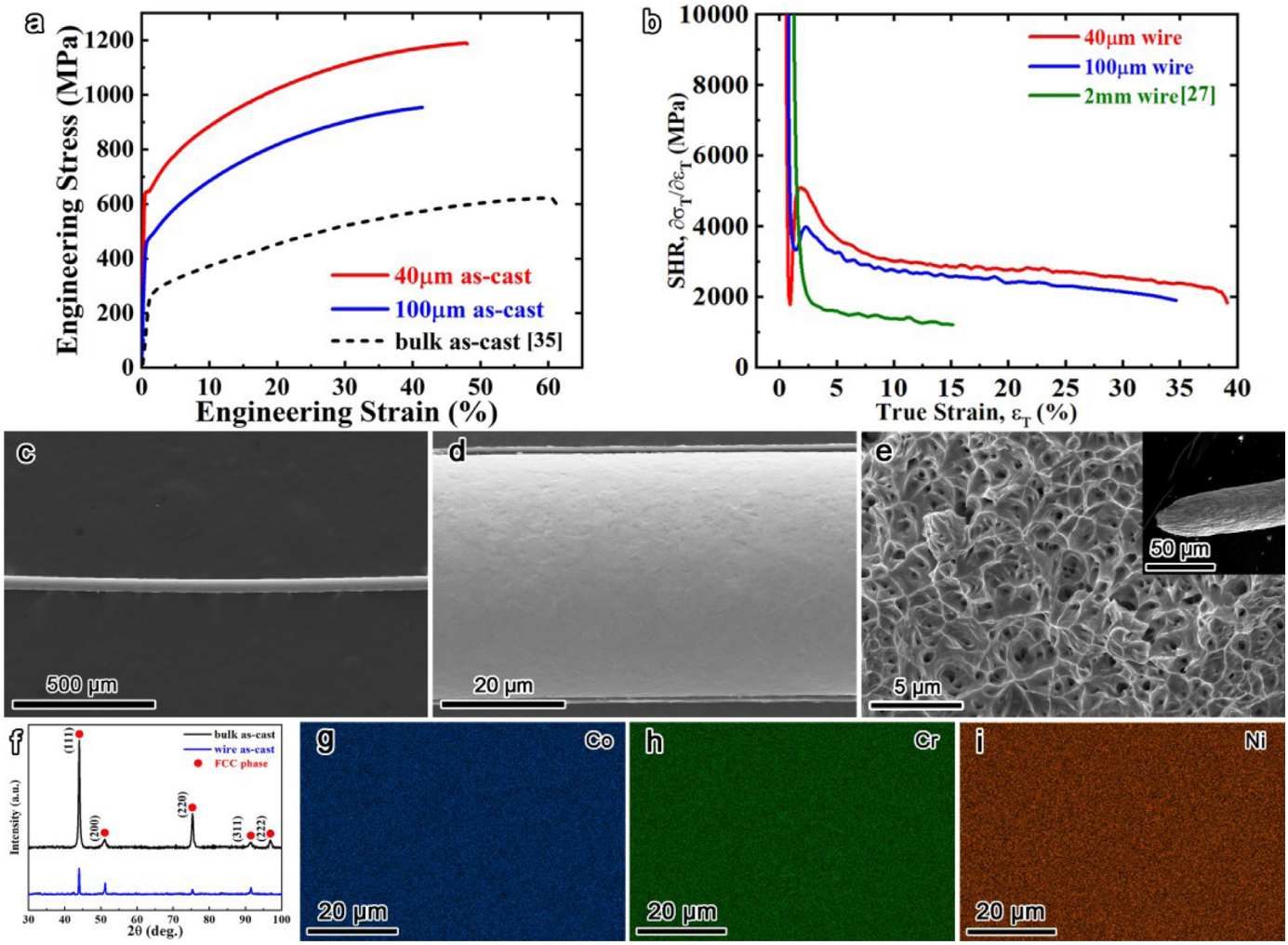

Fig. 1. (a) Tensile engineering stress-strain curves of MEA microwires. (b) Strain hardening rate curves of MEA microwires. SEM images of (c, d) initial MEA microwires, (e) ductile dimpled fracture surface and prominent necking behavior. (f) XRD patterns of the as-cast state of bulk ingot and microwires. (g-i) EDS maps show homogeneous distribution for three elements in microwires.

a strain rate of 1×10^{-4} s^{-1}. Morphology of the microwires was characterized by scanning electron microscope (SEM, JSM-7900F). Phase identification was carried out by SMARTLAB X-ray diffractometer equipped with a Cu K_α radiation source. Average grain size was measured by electron backscattered diffraction (EBSD) using a field emission SEM equipped with EDAX-TSL OIM EBSD system. Structure features were characterized by transmission electron microscope (TEM, JEM-2100F). The focused ion beam (FIB) instrument (Scios2) was applied to the fabrication of EBSD samples and TEM samples.

The measured uniaxial tension stress-strain curves of the CoCrNi microwires are shown in Fig. 1a, where the curve of bulk CoCrNi MEAs in cast condition is also shown for comparison [35]. With a small decrease in ductility, the microwires exhibit much higher strength than the as-cast bulk samples, and considerable improvements both in tensile strength and ductility are achieved with the dimeter reduction. When the diameter of microwires decreases from 100 μm to 40 μm, the yield strength increases from 450 MPa to 638 MPa, the ultimate tensile strength increases from 950 MPa to 1188 MPa and the tensile ductility also increases from 41% to 48%. Both samples show pronounced work-hardening capability (Fig. 1b), which is far beyond that of CoCrNi wire with the diameter of 2mm fabricated by heavily drawing process [27]. Obviously, the MEA microwires exhibit an anomalous size effect, in sharp contrast to conventional single-principal element alloys only showing negligibly minor diameter influence on tension behavior [1]. To uncover the mechanisms underlying the superior properties and the anomalous size effect, the microstructures before and after deformation were characterized in detail.

As shown in Fig. 1c, d, the diameter of initial microwires keeps almost same over a long length. After tensile tests, fully ductile dimpled fracture surface and obvious necking (Fig. 1e) suggesting good plasticity are observed. XRD patterns (Fig. 1f) confirm the single face-centered-cubic (FCC) phase structure of microwires and bulk ingot, and EDS measurements (Fig. 1g-i) reveal the uniform chemical composition both on surface and inside, which indicate the microwires are in a good solid solution state without composition segregation.

According to EBSD images (Fig. 2a, b), both initial microwires have random crystallographic textures, the microstructure is mainly composed of equiaxed grains, and some annealing twins with irregular shape are widely distributed, which together point out that the solidification force rather than the drawing force plays the dominant role in the fabrication of microwires. By statistics, the mean grain sizes (contain annealing twin boundaries) of 40-microwire and 100-microwire are 5.1±1.0 μm and 7.5±1.1 μm, respectively. After tensile tests (Fig. 2c, d), the grains of microwires are severely stretched along tensile direction

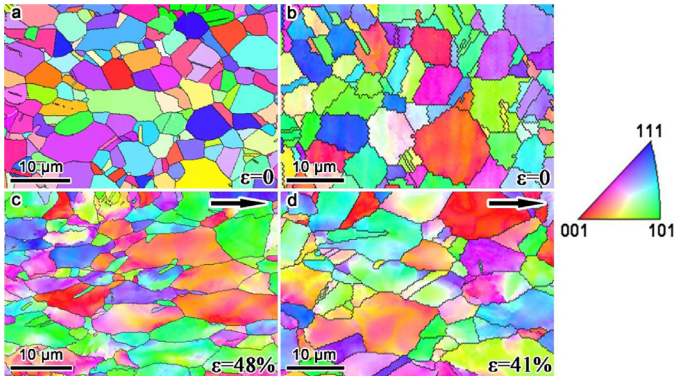

Fig. 2. EBSD images of initial structures of (a) 40-microwire and (b) 100-microwire; deformed structures of (c) 40-microwire with strain of 48% and (d) 100-microwire with strain of 41%.

(black arrow in Fig. 2c, d), among which some deformation twins (DTs) occur. Intra-granular lattice curvatures are developed in almost all grains, and lattice rotations are distinguishable in many grains.

TEM observation was made to further understand deformation mechanisms of microwires. Fig. 3 shows the structure feature of the deformed 100-microwire. First, plenty of stacking faults (SFs) extend in one direction (Fig. 3a), which is related to the very low stacking fault energy (SFE) of CoCrNi alloy (22±4 mJ/m^{-2} [28]). On the one hand, the existence of these SFs increases misorientation in grains, which could possibly evolve into DTs [36] and very fine lamellae structure. On the other hand, it has been reported that further enhancement of work-hardening capacity in CoCrNi is via local phase transformations from FCC to hexagonal close-packed (HCP) that occur along SFs and DTs [31,37]. The formation of high-density DTs (Fig. 3c) and twin lamellae (Fig. 3d) can severely refine grains, providing more boundaries to block dislocation motion and inducing prominent work-hardening capability [38]. No FCC-HCP phase transition is observed in 100-microwire from HREM image and the corresponding selected-area electrical diffraction (SAED) pattern (Fig. 3b).

As the products of interactions between two leading partials from different slip planes, Lomer-Cottrell (L-C) locks widely appear in 100-micron wire (Fig. 3e). Enlarged image as an inset in Fig. 3e represents details of L-C lock, the pentagon with five red dots is the core of L-C locks which is a stair-rod dislocation. It has been reported that the L-C locks have a good capability to accumulate different types of dislocations and a good stability to resist dissociation [39,40]. When the distance between locks is small, high strengthening could be achieved. Thus, the massive formation of L-C locks is very effective in facilitating work hardening in MEA microwires. Besides, when an incoming Shockley dislocations run around L-C locks, twin lamellae would form consequently, which was proposed to be a new twinning mechanism for FCC metals [41].

In addition to aforementioned mechanisms, strong interaction between dense dislocation walls (DDWs) and DTs could also contribute to good work hardening capability (Fig. 3f). Just like nano-twinned copper [42,43], the strong interaction severely subdivides grains, generates numerous internal boundaries, and finally causes dynamic Hall-Patch effect.

In contrast to the 100-microwire, a series of special phenomena have been observed in 40-microwire. The SFs in 40-microwire extend on multiple {111} planes (Fig. 4a). These SFs have a strong interaction with each other, providing more chances for the formation of L-C locks. Much more severe DDWs-DTs interactions are also found in 40-microwire (Fig. 4b). DDWs are typically considered to belong to geometrically necessary boundaries, into which geometrically necessary dislocations (GNDs) are assembled [44,45]. It is worth noting that the average boundary spacing of DDW of 40-microwire is much smaller, corresponding to higher GND density. Aside from above mechanisms, two other unique deformation mechanisms are further observed in 40-microwire.

First, HCP stacking appears, and its thickness could reach eight atomic layers (Fig. 4g-i). Such HCP stacking may act as a favorable site for the growth of HCP phase. It is clear that nanotwins and HCP stacking are distributed in hierarchical structure, and many nanotwin-HCP boundaries are generated. As the transmission of edge dislocations from FCC region into the HCP region would require the activation of some types of dislocations which typically have very large critical resolved shear stress in HCP materials [46], the hierarchical structure and nanotwin-HCP boundaries could act as effective barriers for dislocation slip. Since the HCP stacking has incomplete evolvement and limited quantity, it is not supposed to be the most vital contributing factor for the more superior mechanical properties of 40-microwire.

Secondly, typical bright-field TEM images (Fig. 4c, d) and dark-field TEM images (Fig. 4e, f) show multiple twinning systems. The existence of twinning network could provide adequate pathways for easy glide and enable motion of cross-slip from one boundary to another, so that larger plastic deformation gets coordinated and higher strain hardening capacity is obtained [47,48]. As many twinning systems contain high-density twin lamellae structures, the ductility and strength of 40-microwire could get further enhanced simultaneously.

GNDs represent an extra storage of dislocations required to accommodate the lattice curvature that arises whenever there is a non-uniform plastic deformation [49]. Obvious size effect of strength in traditional metals has been commonly found under micro-torsion, micro-bending, and micro-indentation, but is rare in homogeneous tension [1,49]. According to strain gradient theory, the plastic flow strength increases with diminishing size, and this is attributed to the strengthening effect of strain gradient associated with the GNDs [50–52]. As for MEA microwires, a significant improvement of strength is presented in smaller size even under tension. A question naturally arises: what is the underlying reason for this size effect?

Kernel Average misorientation (KAM) is an OIM analysis tool that characterizes the local misorientation [53], from which the average GND densities are estimated to be 12.3 × 10^{14} m^{-2} and 7.1 × 10^{14} m^{-2} for 40-microwire and 100-microwire at strain ~40% (Fig. 5a, b). This suggests that the deformation of both microwires exhibits a high strain gradient, and the higher tensile strength of 40-microwire can also be ascribed to its higher strain gradient. According to the detailed distribution of GND in both microwires (Fig. 5c), we find that the GND density of 40-microwire is not only higher, but also much more uniform. This uniform distribution of GND may restrict localized deformation, leading to a high work hardening and homogeneous plastic flow capability.

As is known, the MEAs have chemical-disordered structure and non-ignorable lattice distortion [54,55], which become intrinsic sources inducing inhomogeneous deformation or strain gradient even under tension [56]. By contrast, the surface constraint effects [57] are thought to be the extrinsic sources. As shown in Fig. 5d, the cross-section of microwires can be divided into free-surface region and interior region [58]. Assuming that the thickness of free-surface region is d (mean grain size), the volume fraction (f_s) of free-surface region in the whole sample could be described as [59]: $f_s = \frac{4(D-d)d}{D^2}$ ($d < \frac{D}{2}$), where the D represents the diameter of microwires. Then, the f_s are estimated to be 44.5% and 27.8% for 40-microwire and 100-microwire, respectively. This shows that the surface constraint effects would have a non-negligible influence on the mechanical properties of microwires. The work hardening

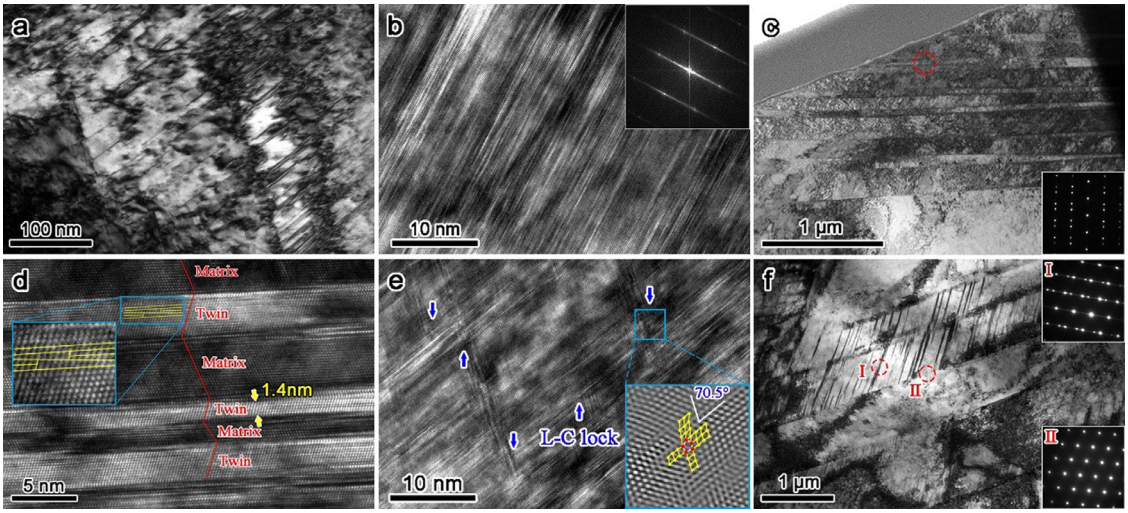

Fig. 3. Detailed microstructure of 100-microwire. Bright-field TEM images of (a) SFs in one direction; (c) high-density DTs; (f) interaction between dislocation and DTs. HREM images of (b) SFs; (d) nanotwin lamellae; (e) L-C locks. All the SAED patterns were taken along [110] zone axis.

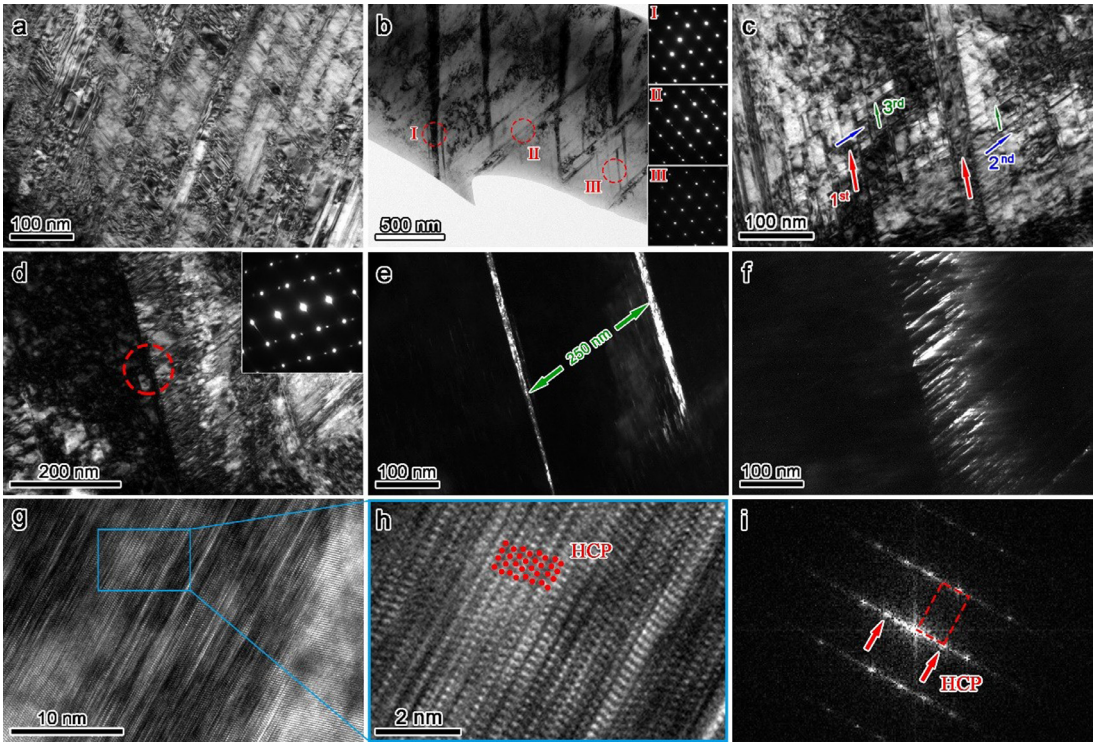

Fig. 4. Detailed microstructure of 40-microwire. Bright-field TEM images of (a) SFs in two directions; (b) much more severe dislocation-DT interaction; (c, d) multiple DTs. Dark-field TEM images of (e, f) multiple DTs. HREM images of (g, h) SFs and HCP stacking, and (i) corresponding SAED pattern. All the SAED patterns were taken along [110] zone axis.

of microwires can be described as: $\Delta\sigma = f_s \cdot \Delta\sigma_s + (1 - f_s) \cdot \Delta\sigma_i$, where the $\Delta\sigma_s$ and $\Delta\sigma_i$ represent the work hardening of free-surface and inner grains. It has been reported that the strength of free-surface grain is weaker with a factor which varies from 0.4 to 0.84 compared to inner grain [60], because the dislocation gliding will not be blocked intensely, and the dislocations can be attracted to surface by image force [61]. Here, an average value of 0.6 was used for calculation. Then, the true stress-strain curves of interior region of microwires are plotted in Fig. 5e.

The higher strain gradient not only results in higher strength, but also an enhancement of ductility by promoting the activation of multiple DTs. The critical stress for twinning (σ_{tw}) in CoCrNi with ultra-fine grain is usually estimated by equation [62,63]: $\sigma_{tw} = \frac{\gamma \cdot b^{-1} + k_{tw}^{HP} \cdot \lambda^{-\frac{1}{2}}}{M}$, where SFE ($\gamma$) is 22mJ/m^2, Burgers vector (b) is 0.252 nm [28], Hall-Petch constant for twinning (k_{tw}^{HP}) is 265 MPa $\cdot$ μm$^{1/2}$ [30], average Schmid factor (M) for FCC is 0.326 [62]. To estimate the critical stress for secondary twinning (σ_{2nd-tw}), the primary twinning spacing, estimated at 250 nm (Fig. 4.e), was regarded as the characteristic length λ. Hence, the σ_{2nd-tw} is roughly estimated to be ~1893 MPa. It is worth noting that the 40-microwire could reach 1893 MPa at true strain ~34% (engineering strain ~40%), but the 100-microwire could only reach 1460 MPa. Therefore, the multiple DTs only appear in 40-microwire. The timely appearance of multiple DTs coordinates more heterogeneous plastic deformation to higher strain and

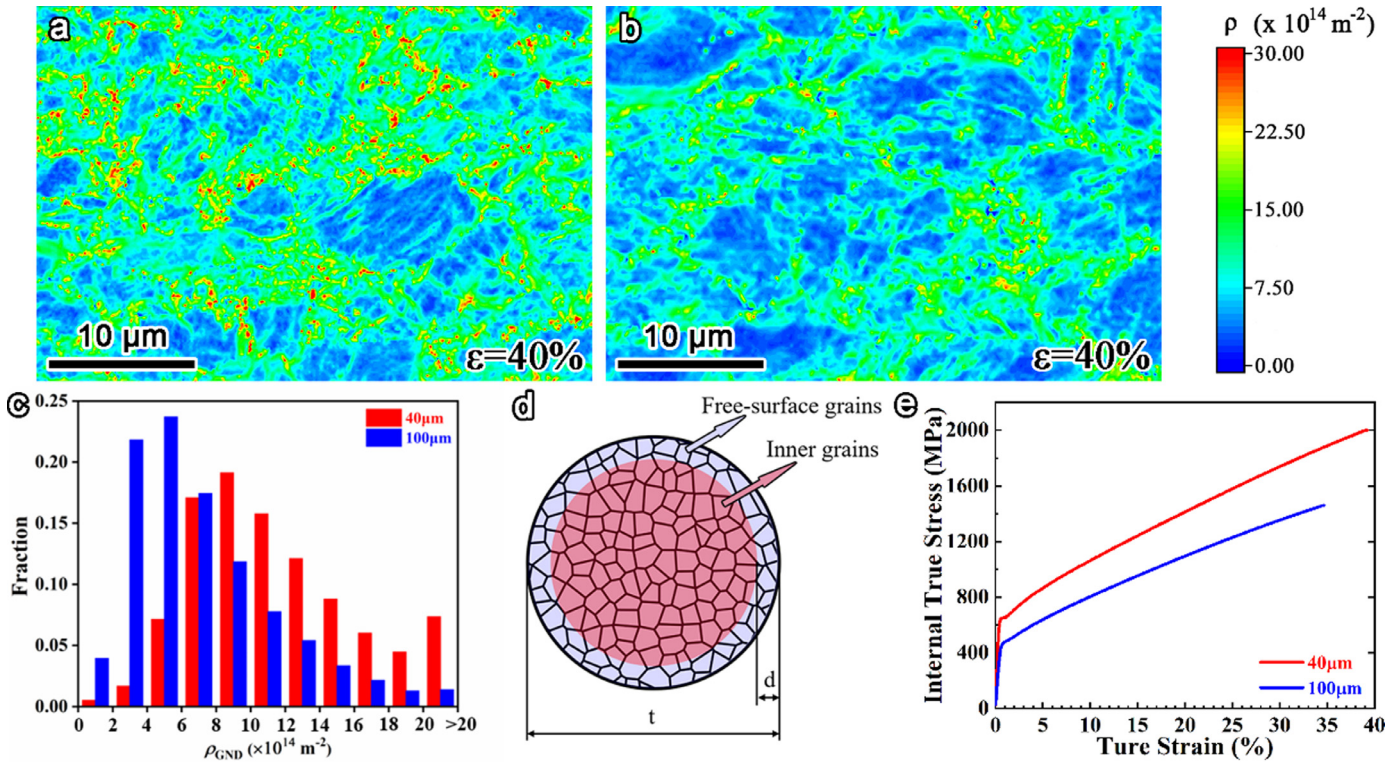

Fig. 5. The GND densities of (a) 40-microwire and (b) 100-microwire with strain of 40% based on the KAM; (c) The distribution of GND density; (d) Schematic of microwires within cross-section; (e) True stress-strain curves of inner grains.

strengthens microwires simultaneously. Thus, the massive activation of multiple DTs accompanied by high-density twin lamellae are thought to be the dominant mechanism for the more superior mechanical properties in 40-microwire.

In conclusion, we successfully fabricated CoCrNi MEA microwires by using Taylor-Ulitovsky method. Excellent combination of strength and ductility was achieved for microwires of two different sizes. Through detailed microstructure characterization, multiple deformation mechanisms were revealed, such as L-C locks, DDWs, DTs and HCP stacking. Furthermore, a surprising size effect was uncovered under tension: the 40 micron-wire shows both higher strength and ductility, which is attributed to the effect of strain gradient associated with the GNDs. The high strain gradient in microwires derived from the intrinsic (i.e., chemical-disorder structure of MEAs) and extrinsic (i.e., surface constraint effects) features promotes the activation of multiple deformation twins, giving rise to both superior strength and ductility in 40-microwire. This work not only sheds light on the micro-mechanism underlying the excellent performance in MEA microwires, but also provides a meaningful guidance for developing new advanced metallic microwires.

Declaration of Competing Interest

We confirm that there is no conflict of interest that could have appeared to affect the work reported in this paper.

Acknowledgments

This work is financially supported by the National Key Research and Development Program of China (No. 2017YFB0702003), the NSFC Basic Science Center Program for “Multiscale Problems in Nonlinear Mechanics” (No. 11988102), the NSFC (Nos. 11790292, 11972346 and 51901235), the Strategic Priority Research Program (No. XDB22040302 and No. XDB22040303), the Key Research Program of Frontier Sciences (Grant No. QYZDJSSW-JSC011), and the Science Challenge Project (No. TZ2018001).

References

[1] N.A. Fleck, G.M. Muller, M.F. Ashby, J.W. Hutchinson, Acta Metall. Mater. 42 (1994) 475–487.
[2] K. Hono, M. Ohnuma, M. Murayama, S. Nishida, A. Yoshie, T. Takahashi, Scr. Mater. 44 (2001) 977–983.
[3] Y. Zhang, M. Li, Y.D. Wang, J.P. Lin, K.A. Dahmen, Z.L. Wang, P.K. Liaw, Adv. Eng. Mater. 16 (2014) 955–960.
[4] Y. Chen, C.A. Schuh, Acta Mater 59 (2011) 537–553.
[5] H. Chen, Y.-D. Wang, Z. Nie, R. Li, D. Cong, W. Liu, F. Ye, Y. Liu, P. Cao, F. Tian, X. Shen, R. Yu, L. Vitos, M. Zhang, S. Li, X. Zhang, H. Zheng, J.F. Mitchell, Y. Ren, Nat. Mater. 19 (2020) 712–718.
[6] J. Yi, X.X. Xia, D.Q. Zhao, M.X. Pan, H.Y. Bai, W.H. Wang, Adv. Eng. Mater. 12 (2010) 1117–1122.
[7] Y. Li, D. Raabe, M. Herbig, P.P. Choi, S. Goto, A. Kostka, H. Yarita, C. Borchers, R. Kirchheim, Phys. Rev. Lett. 113 (2014) 106104.
[8] J. Yeh, S. Chen, S. Lin, J. Gan, T. Chin, T. Shun, C. Tsau, Adv. Eng. Mater. (2004) 299–303.
[9] B. Cantor, I.T.H. Chang, P. Knight, A.J.B. Vincent, Metall. Mater. Trans. A Phys. Metall. Mater. Sci. 377 (2004) 213–218.
[10] Z. Li, S. Zhao, R.O. Ritchie, M.A. Meyers, Prog. Mater. Sci. 102 (2019) 296–345.
[11] E.P. George, D. Raabe, R.O. Ritchie, Nat. Rev. Mater. 4 (2019) 515–534.
[12] F.H. Cao, Y.J. Wang, L.H. Dai, Acta Mater 194 (2020) 283–294.
[13] S. Wei, S.J. Kim, J.Y. Kang, Y. Zhang, Y. Zhang, T. Furuhara, E.S. Park, C.C. Tasan, Nat. Mater. 19 (2019) 1175–1181.
[14] Y. Zhang, T.T. Zuo, Z. Tang, M.C. Gao, K.A. Dahmen, P.K. Liaw, Z.P. Lu, Prog. Mater. Sci. 61 (2014) 1–93.
[15] I. Basu, J.T.M. De Hosson, Scr. Mater. 187 (2020) 148–156.
[16] Y.H. Jo, W.M. Choi, D.G. Kim, A. Zargaran, S.S. Sohn, H.S. Kim, B.J. Lee, N.J. Kim, S. Lee, Sci. Rep. 9 (2019) 1–14.
[17] E. Ma, Scr. Mater. 181 (2020) 127–133.
[18] Z. Li, K.G. Pradeep, Y. Deng, D. Raabe, C.C. Tasan, Nature 534 (2016) 227–230.
[19] Z. Lei, X. Liu, Y. Wu, H. Wang, S. Jiang, S. Wang, X. Hui, Y. Wu, B. Gault, P. Kontis, D. Raabe, L. Gu, Q. Zhang, H. Chen, H. Wang, J. Liu, K. An, Q. Zeng, T.G. Nieh, Z. Lu, Nature 563 (2018) 546–550.
[20] T. Yang, Y.L. Zhao, Y. Tong, Z.B. Jiao, J. Wei, J.X. Cai, X.D. Han, D. Chen, A. Hu, J.J. Kai, K. Lu, Y. Liu, C.T. Liu, Science 362 (2018) 933–937.
[21] J.Y. He, H. Wang, H.L. Huang, X.D. Xu, M.W. Chen, Y. Wu, X.J. Liu, T.G. Nieh, K. An, Z.P. Lu, Acta Mater 102 (2016) 187–196.

[22] B. Gludovatz, A. Hohenwarter, D. Catoor, E.H. Chang, E.P. George, R.O. Ritchie, Science 345 (2014) 1153–1158.
[23] F. Otto, A. Dlouhý, C. Somsen, H. Bei, G. Eggeler, E.P. George, Acta Mater 61 (2013) 5743–5755.
[24] X.F. Liu, Z.L. Tian, X.F. Zhang, H.H. Chen, T.W. Liu, Y. Chen, Y.J. Wang, L.H. Dai, Acta Mater 186 (2020) 257–266.
[25] D. Li, C. Li, T. Feng, Y. Zhang, G. Sha, J.J. Lewandowski, P.K. Liaw, Y. Zhang, Acta Mater 123 (2017) 285–294.
[26] W. Huo, F. Fang, H. Zhou, Z. Xie, J. Shang, J. Jiang, Scr. Mater. 141 (2017) 125–128.
[27] J.P. Liu, J.X. Chen, T.W. Liu, C. Li, Y. Chen, L.H. Dai, Scr. Mater. 181 (2020) 19–24.
[28] G. Laplanche, A. Kostka, C. Reinhart, J. Hunfeld, G. Eggeler, E.P. George, Acta Mater 128 (2017) 292–303.
[29] M. Schneider, E.P. George, T.J. Manescau, T. Záležák, J. Hunfeld, A. Dlouhý, G. Eggeler, G. Laplanche, Int. J. Plast. 124 (2020) 155–169.
[30] S. Yoshida, T. Bhattacharjee, Y. Bai, N. Tsuji, Scr. Mater. 134 (2017) 33–36.
[31] J. Miao, C.E. Slone, T.M. Smith, C. Niu, H. Bei, M. Ghazisaeidi, G.M. Pharr, M.J. Mills, Acta Mater 132 (2017) 35–48.
[32] C.E. Slone, J. Miao, E.P. George, M.J. Mills, Acta Mater 165 (2019) 496–507.
[33] B. Gludovatz, A. Hohenwarter, K.V.S. Thurston, H. Bei, Z. Wu, E.P. George, R.O. Ritchie, Nat. Commun. 7 (2016) 10602.
[34] G.F. Taylor, Phys. Rev. 23 (1924) 655.
[35] Y. Zhou, Q. Li, Z. Xing, R. Zhou, Z. Huang, Y. Huang, W. Guo, Anti-Corrosion Methods Mater 67 (2020) 101–105.
[36] H. Idrissi, L. Ryelandt, M. Veron, D. Schryvers, P.J. Jacques, Scr. Mater. 60 (2009) 941–944.
[37] C. Niu, C.R. LaRosa, J. Miao, M.J. Mills, M. Ghazisaeidi, Nat. Commun. 9 (2018) 1363.
[38] I.J. Beyerlein, X. Zhang, A. Misra, Annu. Rev. Mater. Res. 44 (2014) 329–363.
[39] M. Lederer, V. Gröger, G. Khatibi, B. Weiss, Mater. Sci. Eng. A 527 (2010) 590–599.
[40] Z. Pu, Z.C. Xie, R. Sarmah, Y. Chen, C. Lu, G. Ananthakrishna, L.H. Dai, Philos. Mag. 101 (2021) 154–178.
[41] D. Qi, B. Fu, K. Du, T. Yao, C. Cui, J. Zhang, H. Ye, Scr. Mater. 125 (2016) 24–28.
[42] Q. Pan, H. Zhou, Q. Lu, H. Gao, L. Lu, Nature 551 (2017) 214–217.
[43] K. Lu, L. Lu, S. Suresh, Science 324 (2009) 349–352.
[44] D.A. Hughes, N. Hansen, D.J. Bammann, Scr. Mater. 48 (2003) 147–153.
[45] D. Kuhlmann-Wilsdorf, N. Hansen, Scr. Metall. Mater. 25 (1991) 1557–1562.
[46] J.C. Williams, R.G. Baggerly, N.E. Paton, Metall. Mater. Trans. A Phys. Metall. Mater. Sci. 33 (2002) 837–850.
[47] L. Zhu, S. Qu, X. Guo, J. Lu, J. Mech. Phys. Solids 76 (2015) 162–179.
[48] Z. Zhang, H. Sheng, Z. Wang, B. Gludovatz, Z. Zhang, E.P. George, Q. Yu, S.X. Mao, R.O. Ritchie, Nat. Commun. 8 (2017) 14390.
[49] H. Gao, Y. Huang, Scr. Mater. 48 (2003) 113–118.
[50] L.H. Dai, Z. Ling, Y.L. Bai, Scr. Mater. 41 (1999) 245–251.
[51] N.A. Fleck, J.W. Hutchinson, Adv. Appl. Mech. 33 (1997) 295–361.
[52] W.D. Nix, H. Gao, J. Mech. Phys. Solids 46 (1998) 411–425.
[53] Y. Ateba Betanda, A.L. Helbert, F. Brisset, M.H. Mathon, T. Waeckerlé, T. Baudin, Mater. Sci. Eng. A 614 (2014) 193–198.
[54] Y.Y. Tan, M.Y. Su, Z.C. Xie, Z.J. Chen, Y. Gong, L.R. Zheng, Z. Shi, G. Mo, Y. Li, L.W. Li, H.Y. Wang, L.H. Dai, Intermetallics 129 (2021) 107050.
[55] L.R. Owen, E.J. Pickering, H.Y. Playford, H.J. Stone, M.G. Tucker, N.G. Jones, Acta Mater 122 (2017) 11–18.
[56] J.R. Greer, J.T.M. De Hosson, Prog. Mater. Sci. 56 (2011) 654–724.
[57] P. Lin, Z. Liu, Z. Zhuang, Int. J. Plast. 87 (2016) 32–47.
[58] B. Yang, C. Motz, M. Rester, G. Dehm, L. Forschung, Philos. Mag. 92 (2012) 3243–3256.
[59] H.K. Yang, K. Cao, Y. Han, M. Wen, J.M. Guo, Z.L. Tan, J. Lu, Y. Lu, J. Mater. Sci. Technol. 35 (2019) 76–83.
[60] S.I. Rao, D.M. Dimiduk, M. Tang, T.A. Parthasarathy, M.D. Uchic, C. Woodward, Philos. Mag. 87 (2007) 4777–4794.
[61] M.G.D. Geers, W.A.M. Brekelmans, P.J.M. Janssen, Int. J. Solids Struct. 43 (2006) 7304–7321.
[62] I. Gutierrez-Urrutia, S. Zaefferer, D. Raabe, Mater. Sci. Eng. A 527 (2010) 3552–3560.
[63] M.A. Meyers, O. Vöhringer, V.A. Lubarda, Acta Mater 49 (2001) 4025–4039.